Abdominal Radiology (2019) 44:3377–3387
https://doi.org/10.1007/s00261-019-02201-1

PELVIS

Comparison of MR imaging features of uterine neuroendocrine carcinoma and uterine malignant lymphoma

Michiko Sugimoto[1] · Koichi Koyama[1] · Tomoyuki Ichimura[2] · Taro Shimono[1] · Yasunori Hashiguchi[2] · Yukio Miki[1]

Published online: 31 August 2019

Abstract

Purpose We retrospectively investigated the characteristic magnetic resonance (MR) imaging findings of uterine neuroendocrine carcinoma (UNEC) compared to those of uterine malignant lymphoma (UML).

Methods Nine consecutive female patients with UNEC and 5 female patients with UML participated in this study. MR imaging features were evaluated retrospectively.

Results On MR imaging, seven of 9 UNEC lesions and no UML lesions showed an exophytic growth pattern. All 9 UNEC lesions and no UML lesions showed a growth pattern along the surface of the endocervix or endometrium. Only 1 UNEC lesion and all 5 UML lesions showed diffuse enlargement of the uterus. No UNEC lesions and all 5 UML lesions showed a multinodular shape. These findings showed significant differences between lesions. Findings for margin, endophytic growth pattern, signal intensity, and homogeneity on T2-weighted and T1-weighted imaging did not differ significantly between lesion types. Apparent diffusion coefficient was significantly lower for UML lesions than for UNEC lesions, but was quite low for both types. Local invasion to surrounding tissues was more frequent in UML lesions than in UNEC lesions. There was no significant difference in the frequency of lymphadenopathy between two entities.

Conclusions UNEC lesions tended to show an exophytic growth pattern and growth along the surface of the endocervix or endometrium, even when diffuse enlargement of the uterus was present, while all UML lesions showed a multinodular shape and diffuse enlargement of the uterus without thickening of the cervical epithelium and endometrium.

Keywords Uterine neuroendocrine carcinoma · Uterine malignant lymphoma · Magnetic resonance imaging · Diffusion-weighted imaging · Apparent diffusion coefficient

Introduction

Uterine neuroendocrine carcinoma (UNEC) is rare and shows very aggressive behavior, with rapid growth and frequent metastasis [1, 2]. UNEC arises more frequently from the uterine cervix than from the uterine corpus [2]. UNEC can be categorized into small-cell carcinoma (SmCC) and large-cell neuroendocrine carcinoma (LCNEC), with LCNEC much rarer than SmCC [3, 4]. In addition, UNEC can be classified into pure histological type and mixed type with one or more components of adenocarcinoma, squamous cell carcinoma (SqCC), or other types of carcinoma. UNECs are sometimes difficult to diagnose correctly using only biopsy or cytology for various reasons. First, limited specimens of tissue may result in a diagnosis of other histological subtypes, with morphological small cell-like features such as adenocarcinoma, small-cell variant of SqCC, poorly differentiated carcinoma, sarcoma, melanoma, and lymphoma [3–6]. Second, UNEC is often combined with other histologic tissues as mixed-type UNEC.

Few reports have clarified the magnetic resonance (MR) imaging features of UNECs at the uterine cervix. Duan et al. described UNECs of the cervix as tending to show a homogeneous hyperintense signal on T2-weighted imaging (T2WI), obviously lower apparent diffusion coefficient (ADC), and a higher incidence of lymphadenopathy compared with adenocarcinoma or SqCC, although no significant difference in tumor shape [7]. Yang et al. described

✉ Michiko Sugimoto
m-sugi@med.osaka-cu.ac.jp

[1] Department of Diagnostic and Interventional Radiology, Osaka City University Graduate School of Medicine, 1-4-3 Asahi-machi, Abeno-ku, Osaka, Osaka 545-8585, Japan

[2] Department of Obstetrics and Gynecology, Osaka City University Graduate School of Medicine, Osaka, Japan

UNECs of the cervix as frequently showing both parametrial invasion and lymphadenopathy [8]. Only a small number of case reports have described MR imaging findings for UNECs of the corpus, which show homogeneous or heterogeneous polypoid masses in the endometrial cavity [9–11]. As a result, specific MR imaging features of UNECs of the corpus suitable for facilitating diagnosis have not yet been clarified.

UNECs occasionally infiltrate diffusely into both the parenchyma of the uterine cervix and corpus, and MR imaging findings demonstrate uterine enlargement resembling the appearance of uterine malignant lymphoma (UML) [6, 12–15]. Furthermore, UMLs are also reported to show both a homogeneous hyperintense signal on T2WI and low ADC [15–18], and UMLs easily involve lymph nodes. In addition, UMLs are difficult to diagnose correctly by normal cervical biopsy as well as UNECs, and the direct biopsy of submucosal tumor such as needle biopsy is sometimes necessary [19]. To identify the MR imaging findings between UNECs and UMLs is clinically important, which can lead appropriate biopsy procedure. To the best of our knowledge, no reports have compared MR imaging findings between UNECs and UMLs.

This study investigated whether there are any characteristic MR imaging features of UNECs and whether any differences exist between MR imaging findings for UNECs and UMLs.

Materials and methods

Patient selection

Ten consecutive female patients with pathologically proven UNECs (8 arising from the uterine cervix, 2 from the uterine corpus) and 6 female patients with pathologically proven primary UMLs treated at our hospital between November 2009 and December 2018 were selected for this study. We excluded 1 UNEC patient with the tumor arising from the uterine corpus due to prior chemoradiation therapy for uterine cervical SqCC, and 1 UML patient due to insufficient MR imaging data to detect the lesion. Finally, 9 UNEC patients (UNEC arising from the uterine cervix in 8 and from the uterine corpus in 1) and 5 UML patients were included in this study. The median age of UNEC patients was 41 years (range 24–60 years), and the median age of UML patients was 74 years (range 67–78 years).

The preoperative pathological diagnoses in 9 UNEC patients were as follows: 4 cases were correctly diagnosed, other 4 cases were diagnosed as round cell tumor, undifferentiated carcinoma, SqCC, and adenocarcinoma, respectively, and the other case was diagnosed as SmCC instead of LCNEC. In all 5 patients with UML, biopsy was performed from the uterine cervix. In 2 patients with UML, cervical needle biopsy which is the direct biopsy of tumor [19] was additionally needed for correct diagnosis because the routine cervical biopsy could not provide accurate diagnosis.

Regarding UNEC patients, 8 patients underwent radical hysterectomy with pelvic lymphadenectomy and the other patients received neoadjuvant chemotherapy followed by radical hysterectomy with pelvic and para-aortic lymphadenectomy. All 5 patients with UMLs were diagnosed using biopsy alone, then treated with chemotherapy.

Histopathology

All clinical and histologic characteristics are summarized in Table 1. On histological examination, 3 UNECs were pure-type SmCC, and 6 UNECs were mixed-type SmCC or LCNEC with SqCC and/or adenocarcinoma, or endometrial adenocarcinoma. All 5 UMLs were diagnosed as diffuse large B-cell lymphoma (DLBCL).

MR imaging protocols

Pelvic MR imaging was performed using 1.5-T systems (Achieva; Phillips, Best, the Netherlands; Signa LX or EXCITE; General Electric Healthcare, Milwaukee, WI; or Avanto; Siemens, Erlangen, Germany) or 3.0-T systems (Ingenia or Achieva; Phillips) with a phased-array coil. Axial and sagittal fast spin echo T2WI were obtained with the following parameters: repetition time (TR)/echo time (TE) range 3300–6310/48–120 ms; field of view (FOV), 25–30 cm; slice thickness, 5.0–7.0 mm; interslice gap, 1.0–3.0 mm; matrix, 182 × 352 to 358 × 512. Axial or sagittal fast spin echo T1-weighted imaging (T1WI) was performed using the following parameters: TR/TE range 382–724/7.3–13 ms; FOV, 24–32 cm; slice thickness, 5.0–7.0 mm; interslice gap, 1.0–2.0 mm; matrix, 179 × 320 to 280 × 400. Axial fat-suppressed spin echo T1WI was obtained using the following parameters: TR/TE range 440–850/7.4–11 ms; FOV, 24–32 cm; slice thickness, 5.0–7.0 mm; interslice gap, 1.0–3.0 mm; matrix, 192 × 236 to 258 × 368. Diffusion-weighted imaging (DWI) was performed using a single-shot echo-planar imaging (EPI) sequence with the following parameters: TR/TE, 3500–9000/48–89 ms; FOV, 32–45 cm; slice thickness, 5.0–7.0 mm; interslice gap, 1.0–2.0 mm; matrix, 84 × 128 to 256 × 512; *b* values, 0 and 1000 s/mm^2 or 0, 1000, and

Table 1 Clinical and histologic characteristics of UNECs and UMLs

Age (years)	Primary site	Pathological diagnosis	Clinical stage	pTNM
41	Cervix	SmCC mixed with SqCC	IB1	pT1b2N1M0
51	Cervix	SmCC mixed with adenocarcinoma	IB2	pT1b1N0M0
35	Cervix	SmCC	IIB	pT2bN1M0
42	Cervix	SmCC	IB1	pT1b1N0M0
24	Cervix	SmCC	IB2	pT2bN1M0
41	Cervix	SmCC mixed with adenocarcinoma and SqCC	IB1	pT1b1N1M0
31	Cervix	SmCC mixed with adenocarcinoma	IB1	pT1b1N0M0
60	Cervix	LCNEC mixed with SqCC	IB2	pT2bN1M0
43	Corpus	SmCC mixed with endometrial adenocarcinoma	II	pT2N0M0
78	Cervix-corpus	DLBCL	II	
67	Cervix-corpus	DLBCL	IV	
77	Cervix-corpus	DLBCL	IV	
74	Cervix-corpus	DLBCL	I	
71	Cervix-corpus	DLBCL	I	

The clinical stages were determined using FIGO2008 for UNECs and Lugano classification for UMLs

UNECs uterine neuroendocrine carcinomas, *UMLs* uterine malignant lymphomas, *SmCC* small-cell carcinoma, *SqCC* squamous cell carcinoma, *LCNEC* large-cell neuroendocrine carcinoma, *DLBCL* diffuse large B-cell lymphoma

2000 s/mm^2. Diffusion-weighted images were acquired using the short tau inversion recovery (STIR) technique for fat saturation. ADCs were automatically calculated and displayed on corresponding ADC maps. DWIs were acquired from 8 UNECs and 5 UMLs, and ADC maps were acquired from 6 UNECs and 4 UMLs.

Image analyses

MR images were evaluated by two radiologists (K.K. and M.S. with 22 and 8 years of experience, respectively) blinded to clinical data, and any differences between the two were subsequently resolved in consensus. We evaluated size, signal intensity (intensity on T2WI and T1WI compared with gluteal muscle, homogeneity of signal intensity on T2WI and T1WI, ADCs, and presence of intratumoral hemorrhage defined as hyperintensity on fat-saturated T1WI), shape (irregular/lobulated which is defined as the mass having contour with undulations, ovoid/round or multinodular which is defined as the mass containing multiple nodules), margin (well- or ill-defined), growth pattern (exo- or endophytic growth, growth along the surface of the endocervix or endometrium, diffuse enlargement of the uterus), local invasion (parametrial invasion, direct invasion or dissemination to the adnexa, direct invasion to the bladder or rectum, ureteral dilatation), and other findings (pelvic lymphadenopathy and ascites). Lymph nodes measuring greater than 1 cm in short-axis diameter were considered to be metastatic. To obtain ADCs, after two non-overlapping oval regions of interest (ROIs) were placed manually on the ADC map, mean values were obtained. The size of ROIs was 60–80 mm^2 according to the size of lesions. ROIs were carefully placed in homogeneous and lower ADC regions, but components of hemorrhage were avoided.

Moreover, we compared the MR imaging findings and ADC values of pure-type UNEC lesions with those of mixed-type UNEC lesions.

Statistical analyses

Statistical analyses were performed using EZR version 1.37 statistical software (Jichi Medical University, Saitama, Japan) [20]. Differences between groups were analyzed using Fisher's exact test for categorical valuables and the Mann–Whitney *U* test for continuous variables. Values of $P < 0.05$ were considered statistically significant.

Kappa analysis was used to determine the extent of agreement between the two radiologist observers regarding MR imaging evaluations other than tumor size and ADC. Kappa values were interpreted on the following scale, as suggested by Landis and Koch: kappa value < 0.20, poor agreement; 0.21–0.40, fair agreement; 0.41–0.60, moderate agreement; 0.61–0.80, substantial agreement; and 0.81–1.00, almost perfect agreement [21].

Table 2 Comparison of the clinical and imaging findings between UNECs and UMLs

			UNECs ($n=9$)	UMLs ($n=5$)	P value
Clinical manifestations		Median age (years)	41 (range 24–60)	74 (range 67–78)	0.0033
		Abnormal genital bleeding (yes/no)	7/2	2/3	0.27
MR imaging findings	Size	Median tumor size (mm)	39 (range 20–110)	135 (range 57–179)	0.012
	Signal intensity	Hyperintense/hypointense on T2WI	9/0	5/0	1.0
		Homogeneous/heterogeneous on T2WI	8/1	3/2	0.51
		Iso-hyperintense/hypointense on T1WI	9/0	5/0	1.0
		Homogeneous/heterogeneous on T1WI	9/0	4/1	0.36
		Median ADC ($\times 10^{-3}$ mm^2/sec)	0.630 (range 0.599–0.848)	0.563 (range 0.557–0.607)	0.038
		Presence of intratumoral hemorrhage (yes/no)	1/8	1/4	1.0
	Shape	Irregular, lobulated/ovoid, round	8/1	5/0	1.0
		Multinodular (yes/no)	0/9	5/0	0.0005
	Margin	Well-defined/ill-defined	6/3	2/3	0.58
	Growth pattern	Exophytic growth (yes/no)	7/2	0/5	0.021
		Endophytic growth (yes/no)	5/4	5/0	0.22
		Growth along the surface of the endocervix or endometrium (yes/no)	9/0	0/5	0.0005
		Diffuse enlargement of the uterus (yes/no)	1/8	5/0	0.003
	Invasion	Parametrial invasion (yes/no)	2/7	5/0	0.021
		Invasion or dissemination to the adnexa (yes/no)	0/9	3/2	0.028
		Invasion to the bladder (yes/no)	0/9	3/2	0.028
		Invasion to the rectum (yes/no)	0/9	0/5	1.0
		Ureteral dilatation (yes/no)	0/9	4/1	0.005
Other findings		Pelvic lymphadenopathy > 1 cm on MR imaging (yes/no)	3/6	3/2	0.58
		Pathologically positive pelvic lymph node (yes/no)	5/4	N/A	N/A
		Ascites (yes/no)	6/3	3/2	1.0

UNECs uterine neuroendocrine carcinomas, *UMLs* uterine malignant lymphomas, *N/A* not available

Results

Clinical manifestations, MR imaging findings, and other findings for both UNEC and UML patients are summarized in Table 2.

Clinical manifestations

UNEC patients were significantly younger than UML patients ($P=0.0033$). Abnormal genital bleeding was present in 7 of 9 UNEC patients and 2 of 5 UML patients, showing no significant difference.

MR imaging findings

Median tumor size was significantly smaller for UNEC lesions than for UML lesions ($P=0.012$).

Although the findings of signal intensity and homogeneity on T2WI and T1WI showed no significant differences between UNEC and UML lesions, ADCs were significantly lower in UML lesions than in UNEC lesions ($P=0.038$) (Fig. 1). Intratumoral hemorrhage was present in 1 UNEC lesion (11%) and in 1 UML lesion (20%), again showing no significant difference.

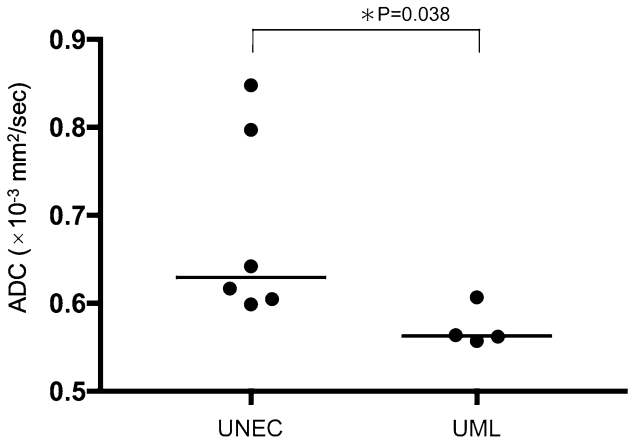

Fig. 1 Scatter plot of ADCs for both UNEC lesions and UML lesions. ADCs of UNEC lesions ranged from 0.599 to 0.848, and those of UML lesions ranged from 0.557 to 0.607. ADCs were significantly lower in UMLs than UNECs ($P=0.038$)

Most UNEC and UML lesions showed irregular or lobulated shape, with no significant difference evident between groups. None of the UNEC lesions showed a multinodular shape, but all UML lesions showed a multinodular shape ($P=0.0005$). Findings for margins showed no significant difference between groups.

Regarding growth pattern, a finding of an exophytic growth pattern was detected only in UNEC lesions (total 7 UNEC lesions among all 9 UNECs; 4 UNEC lesions with only an exophytic growth pattern (representative images, Fig. 2), 3 UNEC lesions with both exophytic and endophytic growth patterns), while no UML lesions showed an exophytic pattern, representing a significant difference ($P=0.021$). On the other hand, the finding of endophytic growth showed no significant difference between UNEC and UML lesions. The pattern of growth along the surface of the endocervix or endometrium was found in all UNEC lesions (representative images, Figs. 2, 3), but no UML lesions showed this pattern, representing a significant difference ($P=0.0005$). The finding of diffuse enlargement of the uterus was found in 1 UNEC lesion (11%) and in 5 UML lesions (100%), indicating a significant difference ($P=0.003$). The only UNEC with the finding of diffuse enlargement of the uterus is shown in Fig. 4. This lesion showed abnormal thickening of the endometrium, whereas all 5 UML lesions showed preservation of the normal cervical epithelium and endometrium (representative images are shown in Fig. 5).

Regarding local invasion, parametrial invasion, invasion or dissemination to the adnexa, direct invasion to the bladder, and ureteral dilatation were found significantly more frequently in UML lesions than in UNEC lesions ($P=0.021$, 0.028, 0.028, 0.005, respectively). Rectal invasion was not detected in both UNEC and UML lesions.

In comparison of pure-type UNEC lesions and mixed-type UNEC lesions, there were no significant differences in the MR imaging findings and ADC values; however, the number of samples was too small to obtain reliable statistical evaluation.

Interobserver agreement regarding MR imaging evaluations except tumor size and ADC was almost perfect ($\kappa=0.811$–1.000).

Other findings

The presence of pelvic lymphadenopathy showed no significant difference between UNEC and UML patients. Pelvic lymphadenopathy was found on MR imaging in 3 UNEC patients, but pathologically positive pelvic lymph nodes were identified in 5 UNEC patients. Ascites showed no significant difference between in UNEC and UML patients.

Discussion

This study assessed MR imaging findings to differentiate UNECs from UMLs. UNEC lesions were revealed to have a tendency to grow along the cervical epithelium or endometrium and to show both exophytic and endophytic growth patterns. All UML lesions showed enlargement of the uterus without an exophytic growth pattern, and the endocervix and endometrium were intact. The presence of exophytic growth and growth along the cervical epithelium or endometrium of UNECs may thus be useful for differentiation from UMLs on MR imaging. Furthermore, a multinodular shape was found in only UML lesions and invasion to adjacent structures was found more frequently in UML lesions. These findings may also be useful for differentiation. Signal intensity on MR imaging was not useful for differentiating UNECs from UMLs. This was attributed to the fact that both UNECs and UMLs tended to show homogeneous intensity on T2WI and T1WI, and both tumors also showed very low ADCs, even though a significant difference existed for ADCs.

At diagnosis, UNECs were significantly smaller than UMLs in our study. When considering that the symptom of abnormal genital bleeding did not show a significant difference between cases, UMLs have already become very large by the time abnormal bleeding appeared, while

abnormal bleeding was found at smaller size in UNEC patients. The reason is thought to be that lesions are exposed on the cervical surface in UNECs, as shown by the pattern of growth along the surface of the endocervix or endometrium in UNECs (100%) in this study.

Both UNEC and UML lesions were more likely to show a homogeneous signal in our study. This is similar to the previous studies [7, 8]. UML lesions are pathologically reported to have less necrosis or bleeding [22]. However,

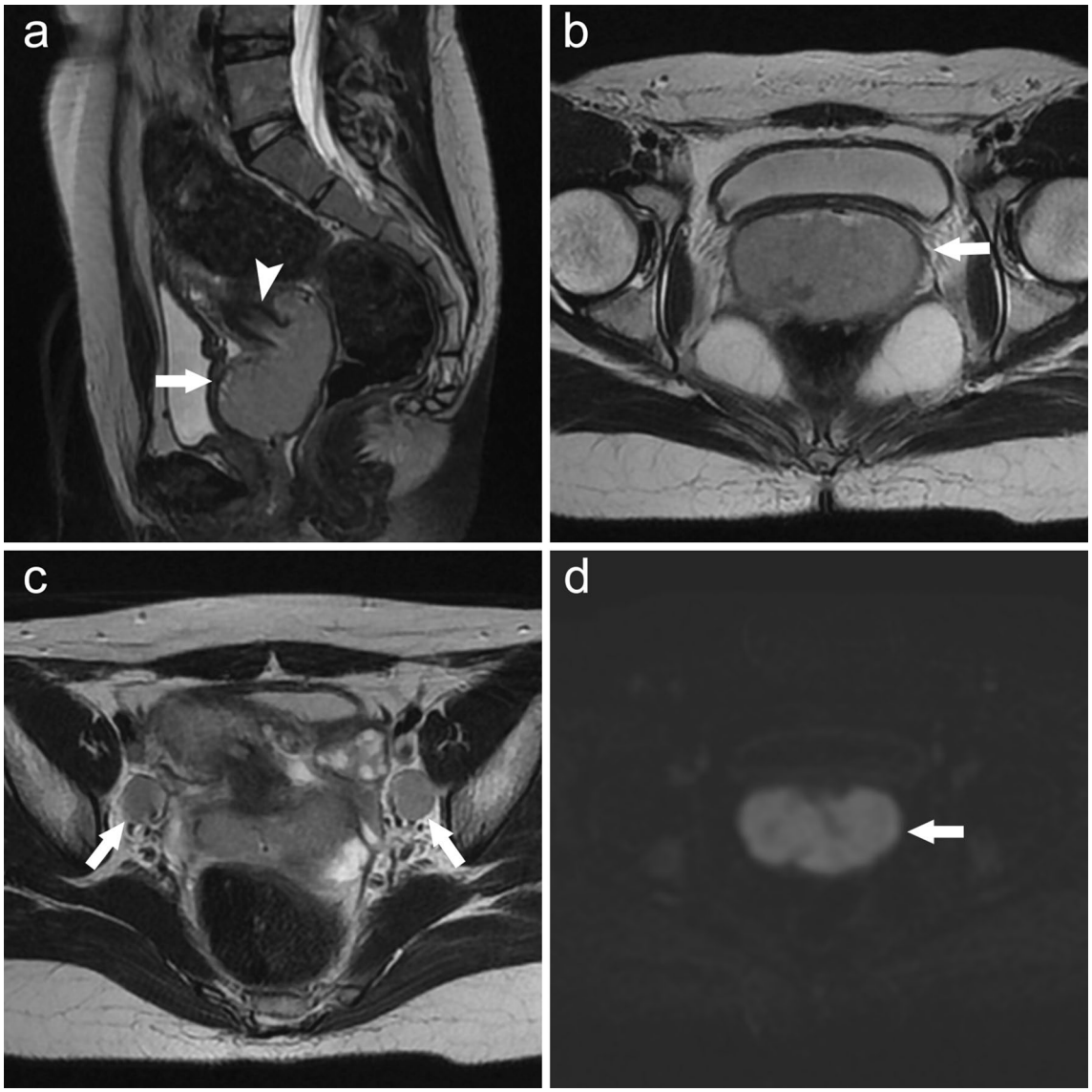

Fig. 2 A 24-year-old woman with neuroendocrine uterine cervical carcinoma (pure-type small-cell carcinoma). Sagittal (**a**) and axial (**b**) T2-weighted images show an exophytic and lobulated mass with a homogeneous hyperintense signal (arrow). The mass grows along the surface of the endocervix (arrowhead). **c** Axial T2-weighted image shows enlarged bilateral obturator lymph nodes (arrow). **d** Axial DWI reveals hyperintensity suggesting restricted diffusion (arrow). ADC map was not available in this patient

Fig. 3 A 41-year-old woman with neuroendocrine uterine cervical carcinoma (small-cell carcinoma mixed with squamous cell carcinoma and poorly differentiated adenocarcinoma). Sagittal (**a**) and axial (**b**) T2-weighted images show an exophytic mass with a homogeneous hyperintense signal along the ectocervix and endocervix without extending to the parametrium (arrow). **c** Axial T2-weighted image shows a left obturator lymph node of normal size, later pathologically confirmed as positive (arrow). **d** Axial DWI shows hyperintensity suggesting restricted diffusion (arrow). **e** Mean ADC is 0.599×10^{-3} mm^2/s (arrow)

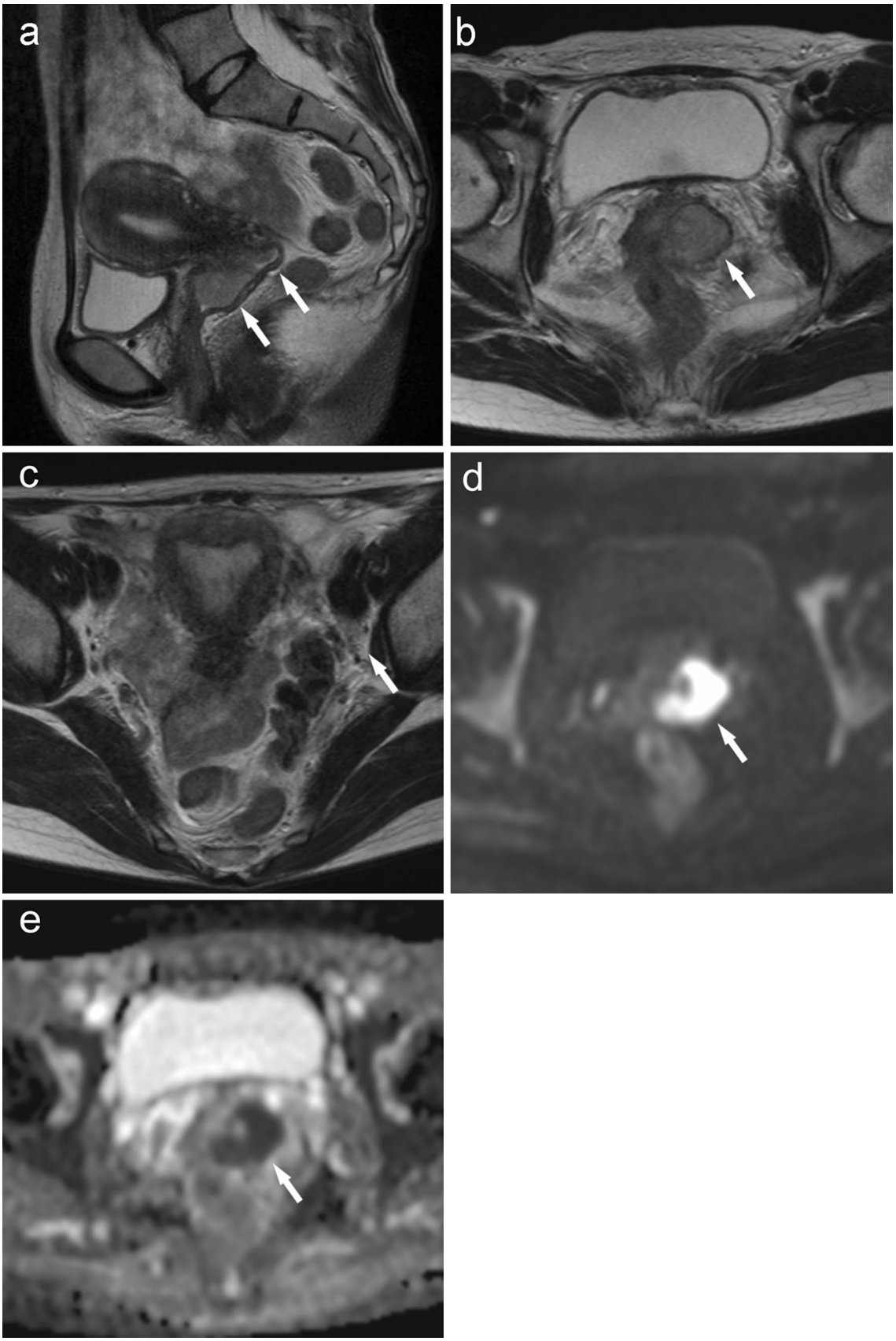
a
b
c
d
e

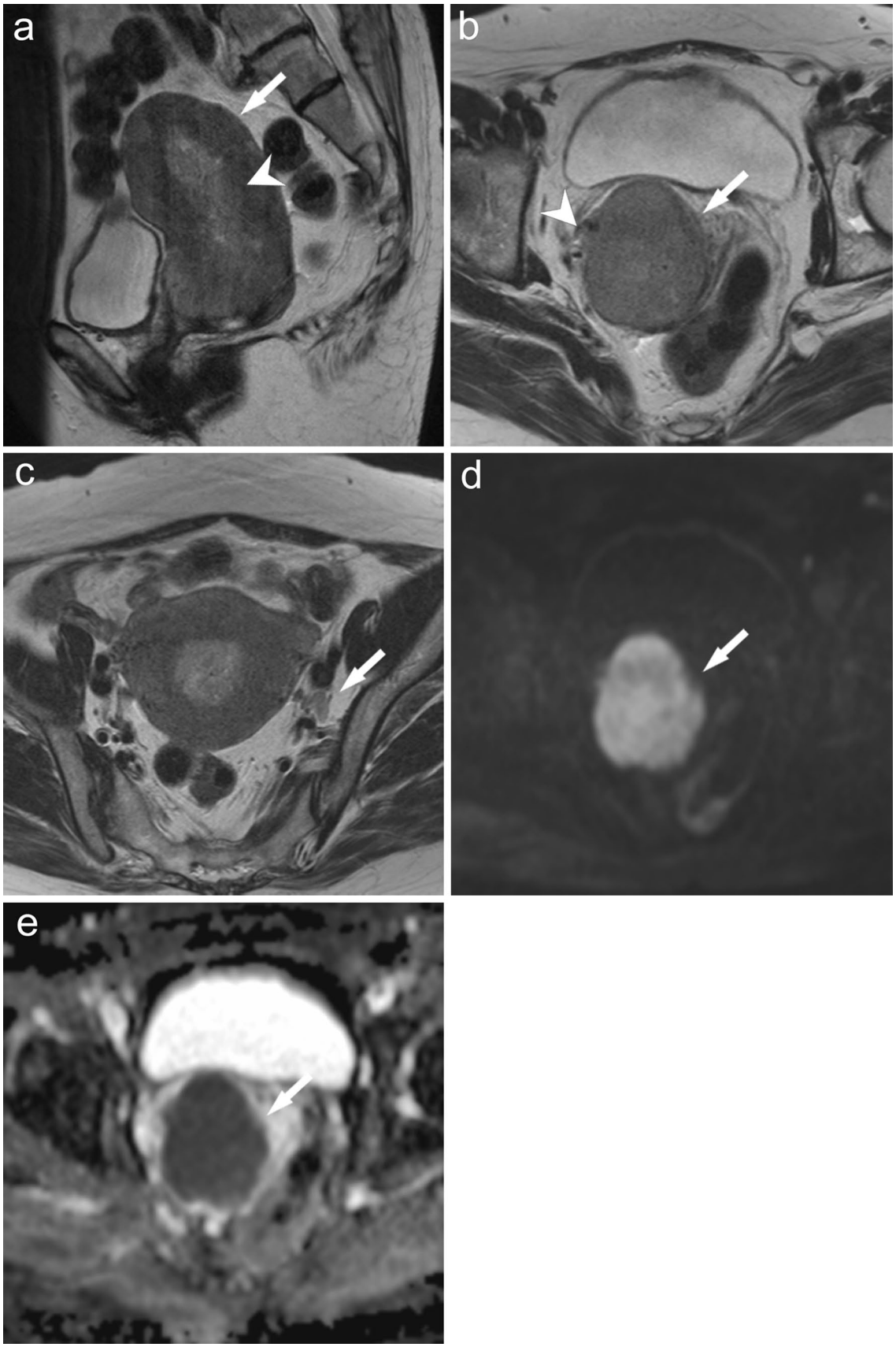
a
b
c
d
e

◂**Fig. 4** A 60-year-old woman with neuroendocrine uterine cervical carcinoma (large-cell neuroendocrine carcinoma mixed with squamous cell carcinoma). **a** Sagittal T2-weighted image shows diffuse enlargement of the uterus, especially of the cervix, which is mimicking uterine malignant lymphoma. The architecture of the uterine corpus is preserved, but invasion and abnormal thickening of the endometrium (arrowhead) are apparent, as well as invasion and thickening of the myometrium (arrow). **b** Axial T2-weighted image shows a well-defined mass in the uterine cervix with a homogeneous hyperintense signal (arrow). The tumor shows slight invasion into the right parametrium (arrowhead). **c** Axial T2-weighted image shows a left obturator lymph node of normal size, later pathologically confirmed as positive (arrow). **d** Axial DWI shows hyperintensity suggesting restricted diffusion (arrow). **e** Mean ADC is 0.642×10^{-3} mm^2/s (arrow)

no pathological rationale for homogeneous signal intensity in UNEC lesions has been shown to date. In our study, UNEC lesions contained a higher percentage of homogeneous lesions than UML lesions, but may be affected by size.

The ADCs of both UNEC and UML lesions were revealed to be quite low in this study. The low ADCs of both tumors reflected hypercellular tumor lesions composed of small round cells [4]. ADCs were significantly lower in UML lesions than in UNEC lesions in this study. Various reasons are thought to contribute to this finding. First, UML lesions themselves are more hypercellular than UNEC lesions. Second, the partial volume effects when setting the ROI may have affected ADCs, because smaller UNEC lesions showed relatively higher ADCs in our study. Third, UML lesions have less necrosis and bleeding within the tumor [22], while coexistence of focal necrosis within dense cell proliferation may be reflected in the ADC in UNEC lesions [4]. Fourth, mixed-type UNECs with other tissue types may lead to higher ADCs. Although a significant difference was seen, ADCs of UNEC and UML lesions are quite low and overlapped, so differentiation using only ADCs seems likely to prove impractical.

Most UNEC lesions had an irregular form and ill-defined margins, but multinodular forms were not found. On the other hand, all UML lesions showed a multinodular morphology. This significant difference in multinodular morphology between UNEC and UML lesions appears useful for differential diagnosis.

UNEC lesions showed both endophytic growth and exophytic growth, and enlargement of the uterus was confirmed in only 1 of the 9 lesions. On the other hand, all UML lesions displayed endophytic growth and enlargement of the uterus, while no exophytic growth was confirmed. The presence of exophytic growth may thus be useful for differential diagnosis. In addition, in a comparison of cases that showed enlargement of the uterus, invasion and thickening of the endometrium were confirmed in UNEC lesions, although these were not confirmed and the endocervix and endometrium were intact in all UML lesions. In fact, UNEC lesions were reported to be able to arise from multipotential basilar epithelial cells, while UML lesions are reported to be uncommon as mucosal lesions and are more often reported as subepithelial and stromal masses [22–25]. The difference between these histopathological findings leads to the difference of MR findings, which could be a clue to the differential diagnosis between UNEC and UML lesions.

Parametrial invasion, direct invasion to the adnexa or bladder, and ureteral dilatation were found more frequently in UML lesions than in UNEC lesions. These are simply attributed due to the larger size of UML lesions.

The frequency of pelvic lymphadenopathy in MR imaging did not show a significant difference between UNEC lesions and UML lesions. Lymphadenopathy is known as a common event in both tumors. In our study of radiological–pathological correlations in UNECs, not only 3 UNEC patients with pelvic lymphadenopathy, but also 2 UNEC patients with normal-sized pelvic lymph nodes revealed lymph node metastases pathologically. In a previous study, the diagnostic accuracy of lymph node metastasis in UNEC patients on MR imaging was reported as low [7]. Furthermore, as many as 57% (4/7) of patients with early-stage UNEC (clinical stage I-IIA) had pelvic lymph node metastases, representing a greater frequency compared with non-UNEC patients in previous reports [7, 26].

Our study has several limitations warranting consideration. First, this study included a relatively small number of cases, because UNECs and UMLs are both rare. Second, MR imaging equipments and protocols for scanning varied, as the study was retrospectively investigated and took place over a prolonged period of 9 years. Third, the contrast-enhanced MR examinations were not evaluated in this study, because they were not performed as routine scanning protocol for uterine tumors at our facility. Fourth, swollen lymph nodes were not always histologically diagnosed, because lymphadenectomy was not performed in all UML cases. Fifth, the number of samples was too small to statistically differentiate MR imaging findings between pure-type UNECs and mixed-type UNECs.

In conclusion, the findings of growth along the cervical epithelium or endometrium and exophytic growth were thought to be useful for differentiating UNECs from UMLs. Even when UNEC lesions showed diffuse

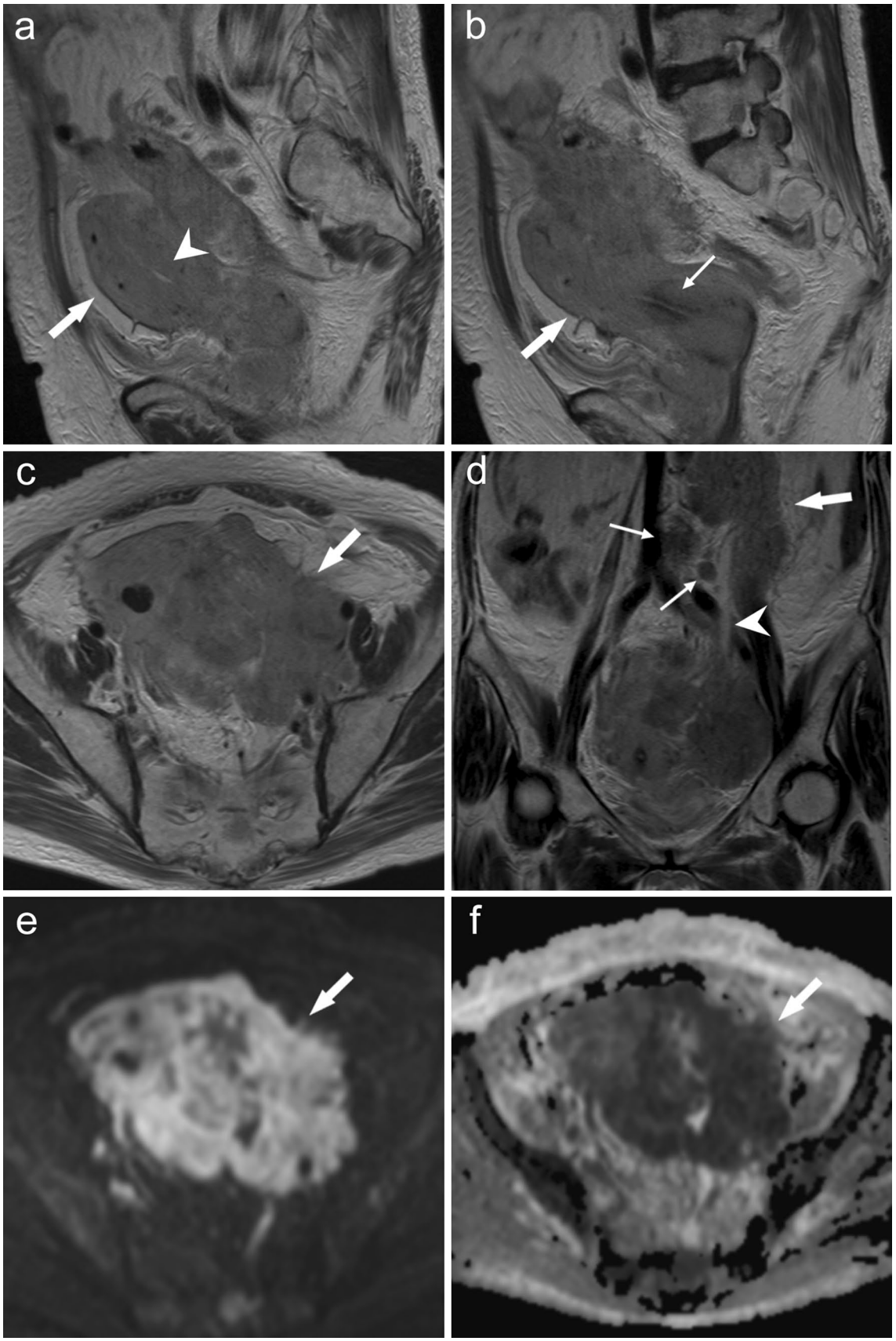
a
b
c
d
e
f

◂**Fig. 5** A 77-year-old woman with uterine malignant lymphoma (diffuse large B-cell lymphoma). Sagittal T2-weighted imaging **a** and **b** shows diffuse enlargement of the uterus with a homogeneous hyperintense signal (arrow). Intact endometrium (arrowhead) and endocervix (thin arrow) are recognized. **c** Axial T2-weighted imaging exhibits a multinodular mass extending beyond uterus with the left adnexal invasion (arrow). **d** Coronal T2-weighted image shows the tumor extending along the left ovarian vein (arrow) and left hydroureter caused by tumor invasion (arrowhead). The enlarged para-aortic and left common iliac lymph nodes are seen (thin arrow). **e** Axial DWI reveals hyperintensity suggesting restricted diffusion (arrow). **f** Mean ADC is 0.607×10^{-3} mm^2/s (arrow)

enlargement of the uterus, as a finding detected in all UML lesions, the exophytic growth and thickening of the endocervix or endometrium appeared useful for ensuring correct diagnosis.

Acknowledgements The authors thank Dr. Shinichi Hamamoto and Dr. Daiju Ueda for their assistance with the production of figures and statistical analysis of data.

Funding No funding was received for this study.

Compliance with ethical standards

Conflict of interest The authors declare that they have no conflict of interest.

Ethical approval This study was approved by the ethics board of our institution (Approval No. 4177), and the requirement to obtain informed consent was waived because of the retrospective design.

References

1. Margolis B, Tergas AI, Chen L, et al (2016) Natural history and outcome of neuroendocrine carcinoma of the cervix. Gynecol Oncol 141(2):247-254
2. Makihara N, Maeda T, Nishimura M, et al (2012) Large cell neuroendocrine carcinoma originating from the uterine endometrium: a report on magnetic resonance features of 2 cases with very rare and aggressive tumor. Rare Tumors 4(3):e37
3. Tempfer CB, Tischoff I, Dogan A, Hilal Z, Schultheis B, Kern P, Rezniczek GA (2018) Neuroendocrine carcinoma of the cervix: a systematic review of the literature. BMC Cancer 18(1):530
4. Howitt BE, Kelly P, McCluggage WG (2017) Pathology of neuroendocrine tumours of the female genital tract. Curr Oncol Rep 19(9):59
5. Dongol S, Tai Y, Shao Y, Jiang J, Kong B (2014) A retrospective clinicopathological analysis of small-cell carcinoma of the uterine cervix. Mol Clin Oncol 2(1):71-75
6. Elsherif S, Odisio EGLC, Faria S, et al (2018) Imaging and staging of neuroendocrine cervical cancer. Abdom Radiol 43(12):3468-3478
7. Duan X, Ban X, Zhang X, et al (2016) MR imaging features and staging of neuroendocrine carcinomas of the uterine cervix with pathological correlations. Eur Radiol 26(12):4293–4302
8. Yang DH, Kim JK, Kim KW, Bae SJ, Kim KH, Cho KS (2004) MRI of small cell carcinoma of the uterine cervix with pathologic correlation. AJR Am J Roentgenol 182(5):1255-1258
9. Tamai K, Koyama T, Saga T, Mikami Y, Fujii S, Togashi K (2007) Small cell carcinoma of the uterine corpus: MR imaging and pathological correlation. J Comput Assist Tomogr 31(3):485-489
10. Tang QL, Liu J, Zuo L, Chi C, Dong HY, Jiang XX, Jiang XF (2017) Bilateral blindness with secondary retinitis pigmentosa following postoperative docetaxel and platinum combination chemotherapy in primary small-cell carcinoma of the endometrium: An unusual case report and review of the literature. Mol Clin Oncol 6(4):477-482
11. Ogura J, Adachi Y, Yasumoto K, et al (2018) Large-cell neuroendocrine carcinoma arising in the endometrium: A case report. Mol Clin Oncol 8(4):575-578
12. Nguyen ML, Han L, Minors AM, Bentley-Hibbert S, Pradhan TS, Pua TL, Tedjarati SS (2013) Rare large cell neuroendocrine tumor of the endometrium: A case report and review of the literature. Int J Surg Case Rep 4(8):651-655
13. Yamamoto T, Maeda M, Mori M, Itch H (2000) MR imaging of small cell carcinoma of the uterus with associated inappropriate secretion of antidiuretic hormone. AJR Am J Roentgenol 174(4):1167-1168
14. Sekine A, Satoh M, Okudela K, et al (2018) Miliary lung metastases from genital large cell neuroendocrine carcinomas. Intern Med 58(8):1127-1130
15. Kido A, Togashi K, Koyama T, Yamaoka T, Fujiwara T, Fujii S (2003) Diffusely enlarged uterus: evaluation with MR imaging. Radiographics 23(6):1423-1439
16. Goto N, Oishi-Tanaka Y, Tsunoda H, Yoshikawa H, Minami M (2007) Magnetic resonance findings of primary uterine malignant lymphoma. Magn Reson Med Sci 6(1):7-13
17. Suzuki Y, Tamaki Y, Hasegawa M, Maebayashi K, Mitsuhashi N (2000) Magnetic resonance images of primary malignant lymphoma of the uterine body: a case report. Jpn J Clin Oncol 30(11):519-521
18. Takeuchi M, Matsuzaki K, Nishitani H (2009) Hyperintense uterine myometrial masses on T2-weighterd magnetic resonance imaging: differentiation with diffusion-weighted magnetic resonance imaging. J Comput Assist Tomogr 33(6):834-837
19. Kawamura N, Ichimura T, Ito F, et al (2002) Transcervical needle biopsy for the differential diagnosis between uterine sarcoma and leiomyoma. Cancer 94(6):1713-1720
20. Kanda Y (2013) Investigation of the freely available easy-to-use software 'EZR' for medical statistics. Bone Marrow Transplant 48(3):452-458
21. Landis JR, Koch GG (1977) The measurement of observer agreement for categorical data. Biometrics 33(1):159–174
22. Harris NL, Scully RE (1984) Malignant lymphoma and granulocytic sarcoma of the uterus and vagina. A clinicopathologic analysis of 27 cases. Cancer 53(11):2530-2545
23. Mandato VD, Palermo R, Falbo A, et al (2014) Primary diffuse large B-cell lymphoma of the uterus: case report and review. Anticancer Res 34(8):4377-4390
24. Frazier SR, Kaplan PA, Loy TS (2007) The pathology of extrapulmonary small cell carcinoma. Semin Oncol 34(1):30-38
25. Yang G, Deisch J, Tavares M, Haixia Q, Cobb C, Raza AS (2017) Primary B-cell lymphoma of the uterine cervix: presentation in Pap-test slide and cervical biopsy. Diagn Cytopathol 45(3):235-238
26. Park JY, Kim DY, Kim JH, Kim YM, Kim YT, Nam JH (2010) Outcomes after radical hysterectomy in patients with early-stage adenocarcinoma of uterine cervix. Br J Cancer 102(12):1692-1698